

This is a repository copy of *First principles investigation of Y2O3-doped HfO2*.

White Rose Research Online URL for this paper:

<http://eprints.whiterose.ac.uk/149210/>

Version: Published Version

Article:

Padilha, Antonio and McKenna, Keith Patrick orcid.org/0000-0003-0975-3626 (2019) First principles investigation of Y2O3-doped HfO2. *Journal of Applied Physics*. 084105. ISSN 0021-8979

<https://doi.org/10.1063/1.5110669>

Reuse

This article is distributed under the terms of the Creative Commons Attribution (CC BY) licence. This licence allows you to distribute, remix, tweak, and build upon the work, even commercially, as long as you credit the authors for the original work. More information and the full terms of the licence here:

<https://creativecommons.org/licenses/>

Takedown

If you consider content in White Rose Research Online to be in breach of UK law, please notify us by emailing eprints@whiterose.ac.uk including the URL of the record and the reason for the withdrawal request.

First principles investigation of Y_2O_3 -doped HfO_2

Cite as: J. Appl. Phys. **126**, 084105 (2019); <https://doi.org/10.1063/1.5110669>

Submitted: 22 May 2019 . Accepted: 25 July 2019 . Published Online: 27 August 2019

A. C. M. Padilha, and K. P. McKenna 

COLLECTIONS

 This paper was selected as an Editor's Pick



View Online



Export Citation



CrossMark

Journal of
Applied Physics

SPECIAL TOPIC:
Polymer-Grafted Nanoparticles

Submit Today!

First principles investigation of Y_2O_3 -doped HfO_2

Cite as: J. Appl. Phys. **126**, 084105 (2019); doi: [10.1063/1.5110669](https://doi.org/10.1063/1.5110669)

Submitted: 22 May 2019 · Accepted: 25 July 2019 ·

Published Online: 27 August 2019



A. C. M. Padilha^{1,2} and K. P. McKenna^{2,a)} 

AFFILIATIONS

¹Brazilian Nanotechnology National Laboratory (LNNano)/CNPEM, Campinas, São Paulo, Brazil

²Department of Physics, University of York, York, Heslington YO10 5DD, United Kingdom

^{a)}Electronic mail: keith.mckenna@york.ac.uk

ABSTRACT

First-principles calculations based on a truncated Coulomb hybrid functional were used to elucidate Y_2O_3 doping of HfO_2 . We calculated the formation enthalpies as well as density of states of nearly 1200 defective structures of two phases of HfO_2 : room-temperature monoclinic and high-temperature cubic structures. For dilute doping, the monoclinic phase is retained and electron trapping states are introduced near the conduction band minimum. For doping concentrations near to 12.5 at. %, the cubic phase is stabilized and the gap is free from charge trapping defect states, making it a suitable high-dielectric constant material for complementary metal-oxide semiconductor applications.

© 2019 Author(s). All article content, except where otherwise noted, is licensed under a Creative Commons Attribution (CC BY) license (<http://creativecommons.org/licenses/by/4.0/>). <https://doi.org/10.1063/1.5110669>

I. INTRODUCTION

HfO_2 is a widely used material in the semiconductor industry as an alternative gate dielectric to SiO_2 . Its large applicability occurs mainly due to the combination of large bandgap and dielectric constant as well as good compatibility with silicon manufacturing technologies.^{1–3} Electronic properties, such as band offsets between HfO_2 and silicon, as well as the properties of intrinsic defects (vacancies and interstitials), impurities, and extended defects have also been well studied.^{4–9} At ambient pressure and temperature, the most stable phase of HfO_2 is monoclinic [space group $P2_1/c$, Fig. 1(a)] with transitions to the tetragonal (space group $P4_2/nmc$) and cubic [space group $Fm\bar{3}m$, Fig. 1(b)] phases at 1022 °C and 2422 °C, respectively.^{2,10} The dielectric constants of the cubic and tetragonal phases are theoretically predicted to be higher than the monoclinic phase, making them more attractive for complementary metal-oxide semiconductor (CMOS) applications.¹¹ This has stimulated a great deal of work aimed at stabilizing the higher temperature phases through doping.¹² Yttrium doping has received particular attention, and successful stabilization of the cubic phase with increased dielectric constant has been demonstrated in many studies.^{12–18} Stabilization of the cubic phase in HfO_2 is observed for Y_2O_3 doping in the range of 4–17 at. %. The emergence of ferroelectricity in both ZrO_2 ¹⁹ and HfO_2 doped with yttrium has also been observed with potential applications in ferroelectric memories.^{19–21}

Analogous to the well known and chemically similar material, yttria stabilized zirconia (YSZ) Y^{3+} ions substitute Hf^{4+} ions in the

lattice and are accompanied by doubly ionized oxygen vacancies to compensate the charge.²² However, the effect of doping on the electronic properties of yttrium-doped HfO_2 remains poorly understood. This is particularly important for CMOS applications where the presence of charge trapping defect states in the gap leads to deleterious effects such as increased leakage current and threshold voltage instability.³ On the other hand, charge trapping materials can be exploited in nonvolatile charge trapping memories for example.²³ For these reasons, a deeper understanding of the electronic properties of yttrium-doped HfO_2 is needed.

In this work, we study Y_2O_3 doping of both monoclinic ($m\text{-HfO}_2$) and cubic ($c\text{-HfO}_2$) hafnium dioxide by means of first-principles density functional theory (DFT) calculations. As noted above, this requires consideration of two types of defects: yttrium ions on hafnium lattice sites (Y_{Hf}') and oxygen vacancies ($\text{V}_{\text{O}}^{\bullet\bullet}$). Real materials will contain a distribution of different local arrangements of the defects and so in our calculations, we characterize the statistical distributions of associated thermodynamic and electronic properties by considering over 1200 distinct defect configurations. We investigate the formation enthalpies of both phases at 3.125 at. %, 6.25 at. %, and 12.5 at. % doping concentrations with respect to pristine $m\text{-HfO}_2$. Examples of such structures are presented in Figs. 1(c) and 1(d). To ensure accuracy of the calculated electronic properties, we employ a nonlocal hybrid functional, which corrects the significant bandgap underestimation of standard local or semilocal approximations to exchange and correlation. Our

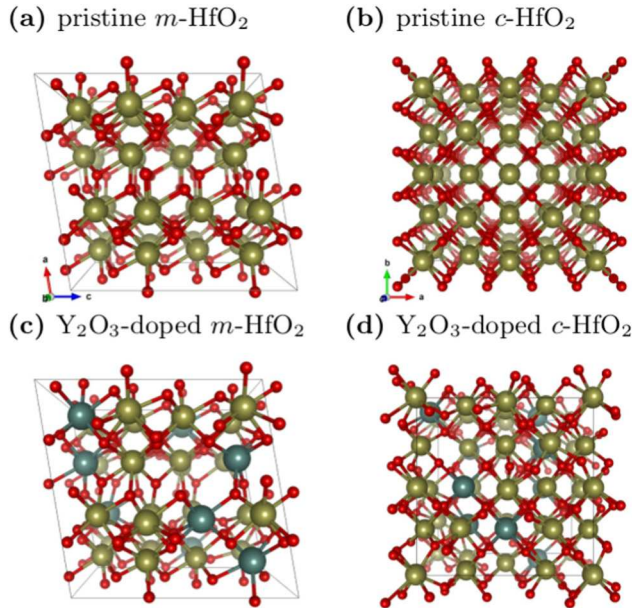


FIG. 1. $2 \times 2 \times 2$ supercells of pristine and Y_2O_3 -doped phases of HfO_2 . (a) Pristine *m*- HfO_2 , (b) pristine *c*- HfO_2 , (c) Y_2O_3 -doped *m*- HfO_2 , and (d) Y_2O_3 -doped *c*- HfO_2 . Gold, gray, and red spheres represent Hf, Y, and O ions, respectively.

results show that stabilization of the *c*- HfO_2 is achieved at 12.5 at. % doping and importantly retains a large bandgap without gap states suitable for CMOS applications. At slightly lower doping concentration where the monoclinic phase is still stable, shallow electron trapping states are introduced near the conduction band minimum.

II. COMPUTATIONAL DETAILS

All calculations in this work were performed using the CP2K package.²⁴ We used the Perdew-Burke-Ernzerhof (PBE) functional²⁵ for structural relaxations and a truncated Coulomb hybrid functional (PBE0-TC-LRC) in order to obtain the density of states (DOS).²⁶ In both cases, the correlation part is approximated using PBE, while for the hybrid calculation, the exchange is given by

$$E_x = (1 - \alpha)E_x^{\text{PBE}} + \alpha \times \begin{cases} E_x^{\text{HF}}, & \text{if } r_{ij} \leq R_c, \\ E_x^{\text{PBE,LRC}}, & \text{if } r_{ij} > R_c, \end{cases} \quad (1)$$

where E_x^{PBE} and $E_x^{\text{PBE,LRC}}$ are the PBE exchange and a long range correction, respectively, while E_x^{HF} is the truncated Hartree-Fock (HF) exchange and r_{ij} is an atomic-center pair distance. The parameters α and R_c that control the amount of HF exchange mixing and the cutoff radius for the truncation of the corresponding exchange²⁶ were 0.25 and 4.0 Å, respectively. In order to perform hybrid calculations in a feasible time, we used the auxiliary density matrix method (ADMM) implemented in CP2K. This

involves projecting the wavefunctions onto a minimal basis of localized orbitals for calculation of the HF integrals, resulting in a significant speed-up of hybrid calculations without significant loss of accuracy.²⁷ This setup guaranteed the reliability of the bandgap for the pristine structures and was employed for all subsequent calculations.

A multigrad comprising 4 levels (cutoffs: 4081, 1360, 454, and 152 eV) was used for the density and convergence criteria for the orbitals and density were both 10^{-6} a.u. (2.7×10^{-5} eV). For the ionic relaxation, single- ζ atomic orbitals were used for both Hf (SZV-MOLOPT-SR-GTH) and O (SZV-MOLOPT-GTH) species, and double- ζ functions were used for Y (DZVP-MOLOPT-SR-GTH). For the DOS calculations, ionic and lattice degrees of freedom were fixed, and double- ζ basis functions were used also for Hf (DZVP-MOLOPT-SR-GTH) and O (DZVP-MOLOPT-GTH) ions. Auxiliary basis functions for the ADMM method were composed of 10 fitted basis for both Hf and Y and 3 fitted basis plus polarization in the case of O atoms. Goedecker-Teter-Hutter pseudopotentials were used for all species (GTH-PBE)²⁸ and Γ -only sampling was performed in reciprocal space.

To sample many distinct defect configurations, for each defect concentrations, we built $2 \times 2 \times 2$ supercells of both *c*- HfO_2 and *m*- HfO_2 , and randomly replaced 2, 4, or 8 Hf atoms by Y atoms, creating $\text{Y}_{\text{Hf}'}$ defects. Next, we created 1, 2, and 4 charge-compensating and $\text{V}_{\text{O}}^{\bullet\bullet}$ defects by randomly removing the corresponding number of oxygen atoms. In this manner, we could model the 3.125 at. %, 6.25 at. %, and 12.5 at. % defect concentrations respectively. The tetragonal phase of HfO_2 is not considered in our study due to the fact that Y-doping in ZrO_2 induces a monoclinic to cubic phase transition, and we expect the same to be true in HfO_2 . For each structure, a PBE relaxation was carried out for both the ion positions and the unit cell vectors (respecting the constraint that the initial symmetry is maintained) up to a tolerance of 4.5×10^{-4} a.u. (1.2×10^{-2} eV Å⁻¹) for the forces and 100 bar for pressure.

The total DOS was obtained using the hybrid functional for all structures relaxed previously. An average DOS $\langle \text{DOS}(\epsilon) \rangle$ was obtained by a Boltzmann-like weighted average

$$\langle \text{DOS}(\epsilon) \rangle = \frac{\sum_i \text{DOS}_i(\epsilon) e^{-E_i/k_B T}}{\sum_j e^{-E_j/k_B T}}, \quad (2)$$

where $\text{DOS}_i(\epsilon)$ is the DOS for the *i*th structure, E_i is the corresponding total energy (relative to ground state), k_B is the Boltzmann constant, and T is the temperature, which was varied from cryogenic (10 K) to room temperature (300 K) up to close to the first transition temperature (1300 K). Relaxations using the PBE functional were also carried out for $3 \times 3 \times 3$ supercells of *m*-, *c*- HfO_2 , and the corundum phase of Y_2O_3 in order to obtain the enthalpy of mixing per formula unit

$$\Delta E_{\text{mix}}(i) = E[\text{Y}_{2i}\text{Hf}_{n-2i}\text{O}_{2n-i}] \quad (3)$$

$$-(n-i)E[\text{HfO}_2] - iE[\text{Y}_2\text{O}_3], \quad (4)$$

where the first term at the right side is the total energy of the defective supercell containing 3.125 at. %, 6.25 at. %, and 12.5 at. % Y concentrations ($i = 1, 2,$ and $4,$ respectively) and the last two terms are the total energies for pristine m -HfO₂ and Y₂O₃.

III. RESULTS

A. Enthalpy of mixing

The enthalpy difference between the undoped cubic and monoclinic HfO₂ per formula unit is 493 meV, while the experimental value is 337(18) meV.²⁹ Even though the predicted value is larger than the experimental value, it presents an error, which is of the same order of the errors from other *ab initio* studies. For example, an enthalpy of 167 meV was obtained by Materlik *et al.* using local density approximation (LDA)³⁰ and of 253 meV by Lee *et al.* using PBE.¹²

Figure 2 shows histograms of the enthalpy of mixing [Eq. (4)] for all defect concentrations and both phases corresponding to the random structures used to model the different concentrations of defects. In both cases, we used the m -HfO₂ phase as the reference energy. In the histograms, two features are noticeable: (i) ΔE_{mix} is always negative for all concentrations in the case of m -HfO₂, while for c -HfO₂, structures start to present a negative ΔE_{mix} only when the doping concentration is at 6.25% or above. (ii) The enthalpy of mixing for both c - and m -HfO₂ becomes very similar when 12.5 at. % doping is reached, i.e., both histograms and corresponding Gaussian fittings present larger overlap between each other than for lower concentrations of doping.

This result suggests that the doping process in this case could lead to a stabilization of the cubic phase of HfO₂. At 3.125 at. %, the two peaks are clearly distinguishable, since the difference between the mean enthalpies of mixing ($\langle \Delta E_m \rangle$ and $\langle \Delta E_c \rangle$) is much larger than the standard deviations (σ) of the distributions ($|\langle \Delta E_m \rangle - \langle \Delta E_c \rangle| \approx 10\sigma$). In the case of 6.25 at. %, this distinction is not as pronounced, but still large enough to separate the two phases, since $|\langle \Delta E_m \rangle - \langle \Delta E_c \rangle| = 4.5\sigma$, and for 12.50 at. %, both

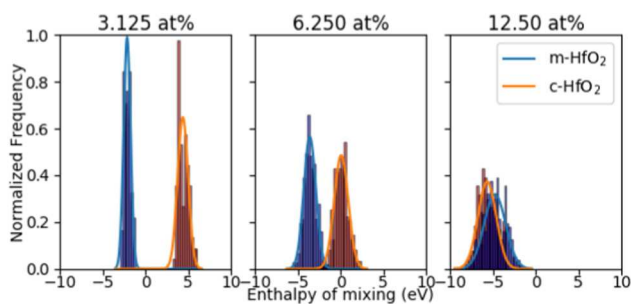


FIG. 2. Histograms of the enthalpy of mixing for both the m -HfO₂ (blue bars) and c -HfO₂ (red bars) for different concentrations of Y₂O₃ doping: left panel 3.125 at. %, central panel 6.25 at. %, and right panel 12.5 at. %. Gaussian curves were fitted for all distributions in order to compare the average values. Around 700 and 500 random structures were generated for m - and c -HfO₂, respectively.

histograms can be considered originated from similar distributions, given that $|\langle \Delta E_m \rangle - \langle \Delta E_c \rangle| = 0.7\sigma$.

B. Electronic properties

For each doping concentration and phase, the most stable structures were selected and the real-space projections of the lowest unoccupied levels [conduction band minima (CBM)] were obtained. Figure 3 shows the projections, where one notices a much more localized character for 6.25% and 12.5% doping levels in the m -HfO₂. For the cubic phase, the same levels are more delocalized, spread over Hf atoms with a clear d character. It is worth pointing out that in the monoclinic structure, oxygen can be 3- or 4-coordinated with the cations, while only 4-coordinated atoms of the same species are present in c -HfO₂. Thus, V_O defects also present the same bonding patterns, and for the larger doping concentrations, a clear localization of the CBM on V_O defects located at the 3-coordinated sites is seen [see Figs. 3(b) and 3(c)].

Average DOS and orbital-projected DOS of both m - and c -HfO₂ are shown in Fig. 4 as well as the same quantity for the pristine structures. Averages were calculated for three temperatures, 10, 300, and 1300 K, showing only small changes in the DOS profiles; thus, we chose to show the results for 300 K only. The pristine DOS of m -HfO₂ exhibits a bandgap of 6.37 eV, while c -HfO₂ presents a value of 6.22 eV. Both values are slightly overestimated with respect to the experimental value of 5.7 eV.³¹

In the case of the monoclinic phase, empty gap states, mainly composed of Hf(d) orbitals, start to populate the vicinity of the conduction band minima (CBM) upon doping, decreasing the bandgap up to ≈ 4 eV for 12.5 at. % doping concentrations. Examples of these levels are shown in Fig. 3. On the other hand, the pristine bandgap of c -HfO₂ is basically preserved upon doping and only a tiny kink corresponding to gap states of the same Hf(d) nature is noticeable close to CBM. This suggests that doping in this case has a negligible impact on the electronic structure of this phase.

IV. DISCUSSION

As noted above, our approach predicts bandgaps for m - and c -HfO₂ (6.4 eV and 6.2 eV), which are slightly overestimated with respect to the experimental value of around 5.7 eV.³¹ Other reports on DFT calculations for HfO₂, however, present much more strongly underestimated values: Koller *et al.* obtained 4.1 eV for m -HfO₂ using PBE³² and Jaffe *et al.* obtained, respectively, 3.8 and 3.7 eV for m - and c -HfO₂ within the generalized gradient approximation (GGA) approximation. Our choice of hybrid functional includes 25% of exact Hartree-Fock exchange. Better agreement with the experimental bandgap could be achieved with a slight reduction in this percentage but should not qualitatively affect any conclusions.

Our results show that at a doping concentration of approximately 12.5 at. % Y₂O₃, it is possible to stabilize the cubic phase of HfO₂. Given the fact that HfO₂ and ZrO₂ present similar chemistries, it is reasonable to expect a similar doping level for the stabilization of the same phase in ZrO₂. In fact, experimental works report a minimum concentration of 7.0–8.5 at. % in this case.³³ We point out that our method does not perform an exhaustive search of possible crystal structures for each

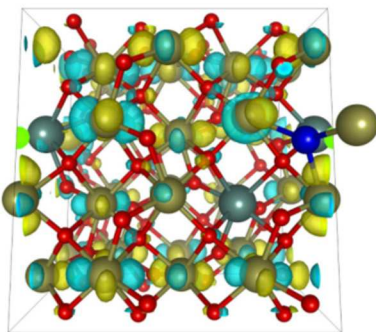
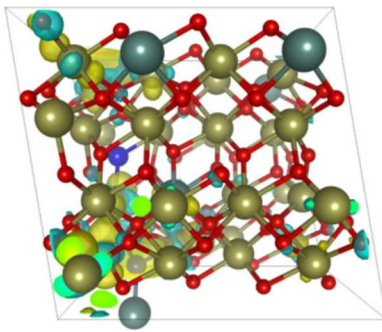
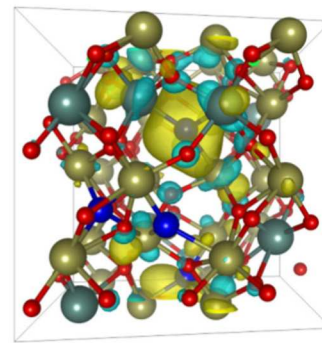
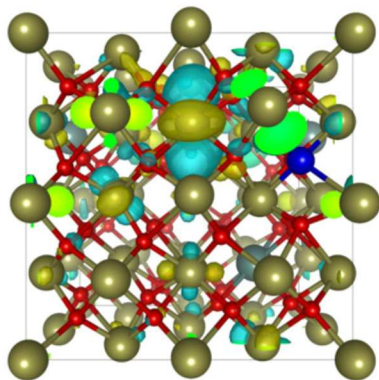
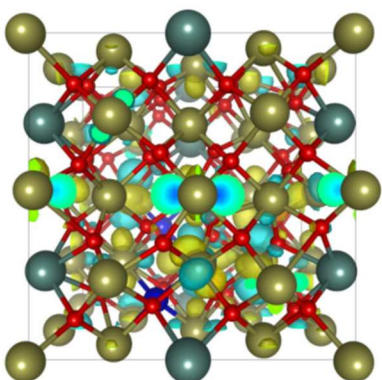
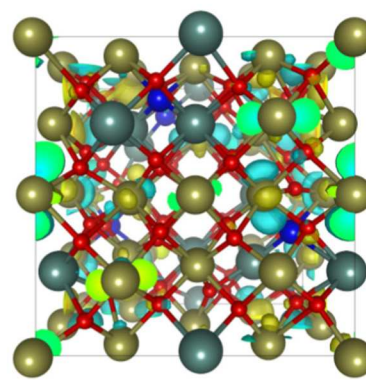
(a) $m\text{-HfO}_2$ 3.125% (side view)(b) $m\text{-HfO}_2$ 6.25% (front)(c) $m\text{-HfO}_2$ 12.5% (top)(d) $c\text{-HfO}_2$ 3.125%(e) $c\text{-HfO}_2$ 6.25%(f) $c\text{-HfO}_2$ 12.5%

FIG. 3. Real-space projections of the first unoccupied level of doped HfO_2 for different doping concentrations. (a) $m\text{-HfO}_2$ with 3.125%, (b) 6.25%, and (c) 12.5%, and (d) $c\text{-HfO}_2$ with 3.125%, (e) 6.25%, and (f) 12.5%. The different colors of the density isosurface represent distinct phases with constant absolute value of 2.5%. Oxygen vacancies are depicted as small blue spheres for clarity.

composition, as in the case of genetic algorithms, and we cannot make any conclusions about the formation of low temperature ordered alloy phases, such as the ones shown by Predith *et al.*³⁴ Nonetheless, visual inspection of the doped structures suggests a uniform localization of the substitutional Y_{Hf} in the most stable cases, while the least stable configurations showed a more clustered arrangement of the same dopants.

To our knowledge, only a few studies of Y-doping of HfO_2 exist in the literature.^{19,30,35} While Muller *et al.* focused on the ferroelectricity of HfO_2 thin films by means of polarization hysteresis measurements and X-ray diffraction data, Chen *et al.* used GGA calculations to study the defect formation energy in $c\text{-HfO}_2$ and possible pressure-driven phase transition from $m\text{-HfO}_2$ to $c\text{-HfO}_2$ upon Y-doping. Their report states that the insertion of substitutional Y into the cubic phase suppresses the detection of an V_{O} -related gap level within the vicinity of the valence band maximum. This observation is in line with our study that points out to the absence of gap levels for the cubic structure for a number of randomly generated structures. On the other hand,

Materlik *et al.* performed a comprehensive first-principles study, using local density approximation (LDA) to the exchange-correlation functional, of the defect chemistry of HfO_2 . They showed that charge-compensating defects such as the ones studied in our work are stable at low oxygen chemical potential. According to their results, there is a competition between the stabilization of the tetragonal phase of HfO_2 , a recently identified ferroelectric phase, and the cubic structure, with a slight tendency (approximately 40 meV lower energy) to the tetragonal phase stabilization at 12.5% doping concentration.³⁰ Here, we considered the cubic phase which was found to be more stable in a different study.¹² We note that such a small difference in energy can arise due to the different methods employed in these studies. Nonetheless, due to the fact that we used a hybrid functional in our calculations for the DOS, we can take a step further and state that no levels close to CBM are detectable in this system as well.

The electronic structure calculations presented in this work are, to our knowledge, the first hybrid-level report about the impact of Y-doping in HfO_2 . Our results show that for $m\text{-HfO}_2$, empty

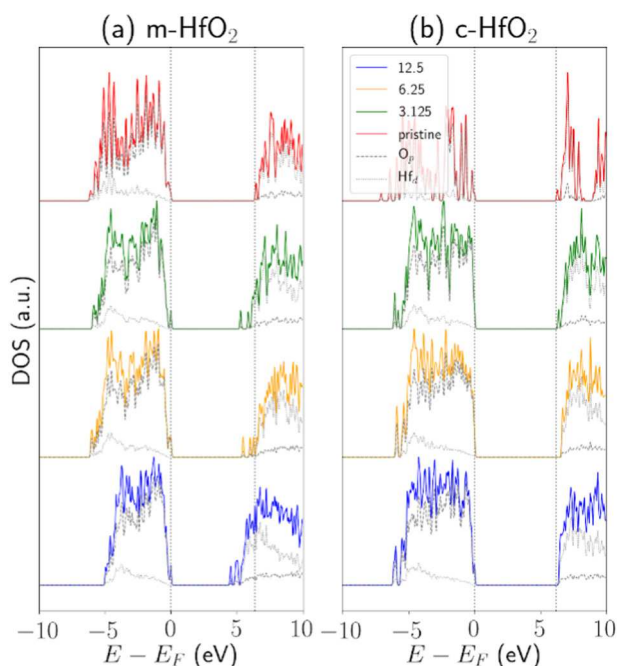


FIG. 4. Total DOS and orbital-projected DOS of the pristine as well as the same quantities averaged for doped *m*-HfO₂ (a) and *c*-HfO₂ (b). All DOS were aligned by the Fermi energy E_F of the pristine phase, and vertical dashed lines depict the bandgap of the corresponding pristine phases. Averages were calculated using a temperature of 300 K.

gap states arise upon doping, while for *c*-HfO₂, no noticeable states are present. These states are mainly donor levels introduced by the doping cation, which were in turn depleted by the charge-compensating vacancies.³⁵ Indeed, our analysis shows a clear localization of the CBM near 3-coordinated V_O defects [see Figs. 3(b) and 3(c)]. We suggest that the states associated with 4-coordinated V_O defects are shifted higher into the conduction band and hence such states are not observed in the gap for the cubic phase. These results confirm that stabilizing the cubic phase with higher dielectric constant by doping with yttrium should be a viable approach for application in CMOS devices.

V. CONCLUSIONS

We have studied Y₂O₃ doping of both *m*- and *c*-HfO₂ by means of hybrid-level DFT calculations on a set of approximately 1200 randomly generated structures. Our results show structural similarities with the already well known system Y₂O₃-doped ZrO₂, which is chemically similar to HfO₂. In both cases, the cubic phase can be stabilized by this kind of doping. Our electronic structure calculations of the defective structures predict the presence of gap levels close to the CBM in *m*-HfO₂, while no such levels are detected in the cubic phase, suggesting the possibility of stabilization of this phase without introduction of charge tapping gap states.

ACKNOWLEDGMENTS

K.P.M. acknowledges support from EPSRC (EP/K003151/1). This work made use of the facilities of Archer, the UK's national high-performance computing service, via our membership in the UK HPC Materials Chemistry Consortium, which is funded by EPSRC (EP/L000202/1). This work also made use of the facilities of N8 HPC Centre of Excellence, provided and funded by the N8 consortium and EPSRC (EP/K000225/1). The Centre is coordinated by the Universities of Leeds and Manchester.

All data created during this research are available by request from the University of York Research database <http://dx.doi.org/10.15124/6af02367-39f8-4577-bcd9-4bd7bd0f9e77>.

REFERENCES

- G. D. Wilk, R. M. Wallace, and J. M. Anthony, "High- κ gate dielectrics: Current status and materials properties considerations," *J. Appl. Phys.* **89**, 5243–5275 (2001).
- J. Choi, Y. Mao, and J. Chang, *Mater. Sci. Eng. R* **72**, 97–136 (2011).
- J. Robertson, "New high- k materials for CMOS applications," *Compr. Semicond. Sci. Technol.* **1–6**, 132–176 (2011).
- A. C. M. Padilha and K. P. McKenna, *Phys. Rev. Mater.* **2**, 045001 (2018).
- K. P. McKenna and D. M. Ramo, *Phys. Rev. B* **92**, 205124 (2015).
- S. R. Bradley, K. P. McKenna, and A. L. Shluger, "The behaviour of oxygen at metal electrodes in HfO₂ based resistive switching devices," *Microelectron. Eng.* **109**, 346–350 (2013).
- K. McKenna, A. Shluger, V. Iglesias, M. Porti, M. Nafria, M. Lanza, and G. Bersuker, "Grain boundary mediated leakage current in polycrystalline HfO₂ films," *Microelectron. Eng.* **88**, 1272–1275 (2011).
- T. V. Perevalov, V. S. Aliev, V. A. Gritsenko, A. A. Saraev, and V. V. Kaichev, "Electronic structure of oxygen vacancies in hafnium oxide," *Microelectron. Eng.* **109**, 21–23 (2013).
- W. Zhang and Z. F. Hou, "Interaction and electronic structures of oxygen divacancy in HfO₂," *Phys. Status Solidi Basic Res.* **250**, 352–355 (2013).
- J. E. Jaffe, R. A. Bachorz, and M. Gutowski, *Phys. Rev. B* **72**, 1–9 (2005).
- X. Zhao and D. Vanderbilt, "First-principles study of structural, vibrational, and lattice dielectric properties of hafnium oxide," *Phys. Rev. B* **65**, 233106 (2002).
- C.-K. Lee, E. Cho, H.-S. Lee, C. S. Hwang, and S. Han, *Phys. Rev. B* **78**, 012102 (2008).
- J. Niinistö, K. Kukli, T. Sajavaara, M. Ritala, M. Leskelä, L. Oberbeck, J. Sundqvist, and U. Schröder, "Atomic layer deposition of high-permittivity yttrium-doped HfO₂ films," *Electrochem. Solid-State Lett.* **12**, G1–G4 (2009).
- M. Komatsu, R. Yasuhara, H. Takahashi, S. Toyoda, H. Kumigashira, M. Oshima, D. Kukuruznyak, and T. Chikyow, "Crystal structures and band offsets of ultrathin HfO₂-Y₂O₃ composite films studied by photoemission and x-ray absorption spectroscopies," *Appl. Phys. Lett.* **89**, 172107 (2006).
- Q. Tao, G. Jursich, P. Majumder, M. Singh, W. Walkosz, P. Gu, R. Klie, and C. Takoudis, "Composition-structure-dielectric property of yttrium-doped hafnium oxide films deposited by atomic layer deposition," *Electrochem. Solid-State Lett.* **12**, G50–G53 (2009).
- L. Shi, Y. Zhou, J. Yin, and Z. Liu, "Characterization upon potential properties of HfO₂ stabilized by Y₂O₃ films as cubic phase," *J. Appl. Phys.* **107**, 014104 (2010).
- Z. K. Yang, W. C. Lee, Y. J. Lee, P. Chang, M. L. Huang, M. Hong, K. L. Yu, M.-T. Tang, B.-H. Lin, C.-H. Hsu, and J. Kwo, "Structural and compositional investigation of yttrium-doped HfO₂ films epitaxially grown on Si (111)," *Appl. Phys. Lett.* **91**, 202909 (2007).
- T. Roessler, J. Gluch, M. Albert, and J. Bartha, "Electrical characterisation of HfYO MIM-structures deposited by ALD," *Thin Solid Films* **518**, 4680–4683 (2010).

- ¹⁹J. Müller, U. Schröder, T. S. Bösccke, I. Müller, U. Böttger, L. Wilde, J. Sundqvist, M. Lemberger, P. Kücher, T. Mikolajick, and L. Frey, "Ferroelectricity in yttrium-doped hafnium oxide," *J. Appl. Phys.* **110**, 114113 (2011).
- ²⁰T. Shimizu, K. Katayama, T. Kiguchi, A. Akama, T. J. Konno, O. Sakata, and H. Funakubo, *Sci. Rep.* **6**, 32931 (2016).
- ²¹S. Clima, D. J. Wouters, C. Adelman, T. Schenk, U. Schroeder, M. Jurczak, and G. Pourtois, *Appl. Phys. Lett.* **104**, 092906 (2014).
- ²²J. W. Fergus, *J. Power Sources* **162**, 30–40 (2006).
- ²³C. Zhao, C. Z. Zhao, S. Taylor, and P. R. Chalker, "Review on non-volatile memory with high-k dielectrics: Flash for generation beyond 32 nm," *Materials (Basel)* **7**, 5117–5145 (2014).
- ²⁴J. Hutter, M. Iannuzzi, F. Schiffmann, and J. Vandevondele, *Wiley Interdiscip. Rev. Comput. Mol. Sci.* **4**, 15–25 (2014).
- ²⁵J. P. Perdew, K. Burke, and M. Ernzerhof, *Phys. Rev. Lett.* **77**, 3865–3868 (1996).
- ²⁶M. Guidon, J. Hutter, and J. Vandevondele, "Robust periodic Hartree-Fock exchange for large-scale simulations using Gaussian basis sets," *J. Chem. Theory Comput.* **5**, 3010–3021 (2009).
- ²⁷M. Guidon, J. Hutter, and J. Vandevondele, *J. Chem. Theory Comput.* **6**, 2348–2364 (2010).
- ²⁸S. Goedecker and M. Teter, "Separable dual-space Gaussian pseudopotentials," *Phys. Rev. B* **54**, 1703–1710 (1996).
- ²⁹T. A. Lee and A. Navrotsky, "Enthalpy of formation of cubic yttria-stabilized hafnia," *J. Mater. Res.* **19**, 1855–1861 (2004).
- ³⁰R. Materlik, C. Künneth, M. Falkowski, T. Mikolajick, and A. Kersch, "Al-, Y-, and La-doping effects favoring intrinsic and field induced ferroelectricity in HfO₂: A first principles study," *J. Appl. Phys.* **123**, 164101 (2018).
- ³¹M. Balog, M. Schieber, M. Michman, and S. Patai, *Thin Solid Films* **41**, 247–259 (1977).
- ³²D. Koller, F. Tran, and P. Blaha, *Phys. Rev. B* **85**, 155109 (2012).
- ³³V. V. Kharton, E. N. Naumovich, and A. A. Vechev, *J. Solid State Electrochem.* **3**, 61–81 (1999).
- ³⁴A. Predith, G. Ceder, C. Wolverton, K. Persson, and T. Mueller, "Ab initio prediction of ordered ground-state structures in ZrO₂–Y₂O₃," *Phys. Rev. B* **77**, 1–7 (2008).
- ³⁵G. H. Chen, Z. F. Hou, X. G. Gong, and Q. Li, "Effects of Y doping on the structural stability and defect properties of cubic HfO₂," *J. Appl. Phys.* **104**, 074101 (2008).